Available online at www.sciencedirect.com
SCIENCE DIRECT®
Journal of Magnetic Resonance 163 (2003) 23–37
JMR Journal of Magnetic Resonance
www.elsevier.com/locate/jmr

Simplified model and stabilization of SSFP sequences

Patrick Le Roux*

GE Medical Systems, Applied Science Lab Europe, 283 rue de la Miniere, Buc Cedex 78530, France

Received 19 November 2002; revised 13 February 2003

Abstract

Steady-state free precession (SSFP) is used today in a form similar to other rapid sequences like fast spin echo (FSE) where a large longitudinal magnetization is present at the beginning of the train of excitations. This results in a transient behavior which impedes any measurement before the steady state is established. Several solutions have been proposed to stabilize the signals more quickly. Starting from a simplified model of signal generation, and by a suitable change of reference frame, this paper justifies theoretically the linear ramp-up proposed by Nishimura and Vasanawala (p. 301, 8th Annual Proceedings of ISMRM, 2000, Denver). This linear ramp-up can be generalized into a one giving less oscillatory residues. The solution is efficient in the sense that it does not require nutation angles larger than the one used during the stabilized period. Also, this solution is robust because it scales up or down nicely and is thus insensitive to B_1 variations.

Keywords: Steady state free precession; Fast spin echo; Relaxation; Stabilization; True FISP

1. Introduction

Typically the steady state free precession (SSFP) sequence has been used in a 3D mode with a steady state established well before the beginning of the signal acquisition. Classically the sequence was also used in a dispersed (or crushed) mode where a large constant gradient integral is created in the interval TR (repetition time) between two consecutive pulses. Recently new development has been generated by the rediscovery [1] of the true-FISP method [2] (or refocused SSFP) where all the gradient integrals between two consecutive excitations are nulled. This results in a large signal, but also in a sensitivity to chemical shift or main field homogeneity, and it is the reason why the sequence was rediscovered only when the progress in gradient technology could shorten the repetition time below a few milliseconds. The high contrast obtained between fluids and organs renders the sequence suitable for cardiac imaging [3,4], and one would certainly prefer in this context to use a 2D mode because of the shorter minimum acquisition time it permits. Unhappily the time necessary to reach the dynamic equilibrium by relaxation only is prohibitive. This has been addressed by relatively simple solutions [1], but in the recent years a more elaborate solution [5,6] based on a sequence of variable pulse angles determined by the Shinnar–Le Roux algorithm [7] has been proposed. The aim of this preparation is to transfer, for each resonance frequency, the initial longitudinal magnetization toward its steady state position. Putting aside the difficulty for a non-specialist to understand this sort of design, it is not certain that this solution is robust against B_1 gain setting errors or lack of homogeneity as pointed out in [5]. There is another interesting approach presented in [8] which uses a simple linear ramp up of the nutation angle. The linear system framework used by the authors of [8] to introduce their proposal is questionable in a context of nutation angles ranging from 0° to 60° in the course of 10 pulses, that is to say with some magnetization elements undergoing more than one complete rotation. One will see that one can justify the solution of [8] by putting oneself in a new reference frame where a linear approximation becomes valid. Once this is done, the linear ramp is justified in a large part, but also a more efficient solution naturally comes to mind, based on classical linear filter design. The end result is not as good as the best theoretically

* Fax: +33-1-3070-4639.
E-mail address: Patrick.LeRoux@med.ge.com.

1090-7807/03/$ - see front matter © 2003 Elsevier Science (USA). All rights reserved.
doi:10.1016/S1090-7807(03)00115-0

imaginable SLR design, but is very insensitive to B_1 setting errors.

The solution proposed here is relatively easy to develop once a model for the signal generation in SSFP or FSE has been introduced. Despite the fact that the aim of this article is the stabilization of SSFP, it will give some results or remarks pertaining to FSE and also introduce some simplified equations describing relaxation in both type of sequences. These simplified equations are valid only when a set of Bloch equations with a three dimensions state vector representing magnetization is acceptable. These Bloch equations describe the longitudinal and transversal processes empirically, by a first order process (with time constant T_1 and T_2). In addition, the simplified model is valid only if the transverse relaxation time constant T_2 is long in comparison to the time interval separating two RF pulses. There is no question to describe exchange, coupling, or diffusion in strong local fields and certainly not any solid NMR phenomenon with this simple model. Flow, or movement is not taken into account in this article. Although it is made use of spinors when deriving the rotation from echo to echo, this is only used as an efficient mathematical tool for describing (classical) rotations and does not refer to any quantum mechanics formalism. The model so obtained is able to approximately predict the magnetization behaviour when the excitation is a train of constant nutation pulses. In a subsequent step, a simplified model of the magnetization dynamics, applicable when the nutation angle of the pulses varies slowly, is developed. This gives some insight of what a true, numerical, resolution of the Bloch equations would permit to obtain. This is in order to be able to synthetize nutation angles modulations which generate stable echo signals. To verify this synthesis step, the original, non-simplified Bloch equation will be used.

2. Simple model of signal generation in SSFP

The only rigorous approach in presence of relaxation processes is to proceed as in [5]: after having characterized the magnetization M by a three real values $M = (x, y, z)^{\mathrm{t}}$ one writes the linear invariant dynamic system (represented by a 3×3 real matrix) which links the value of the state vector M_{k-1} before the kth pulse to the value M_k it has before the next pulse: $M_k = AM_{k-1} + B$. The matrix A represents first the succession of rotations applied by the γb_0 and γb_1 fields, the cycle rotation, and secondly the transverse and longitudinal relaxations. The vector B represents the longitudinal recovery. One can choose a cycle beginning just before one RF pulse and ending just before the next RF pulse, but one may choose any other cycle of duration one repetition time. We indeed note that knowing the magnetization at one time in the precession interval permits to know this magnetization everywhere in the precession interval. Indeed the evolution is then a rotation around the z axis, with a transverse relaxation and a T_1 recovery along z, and all these operations can be easily written in an analytical form. Being a standard stationary linear dynamic system of low order, this system can be studied relatively easily and the equilibrium values can be found in analytical manner [9]. Nevertheless the rather complicate mathematical expression tends to impede the comprehension of the physical phenomena. The complication comes from the relaxation processes. In presence of relaxations the magnetization tends towards a dynamic equilibrium intermediary between the axis of the cycle rotation and the axis z along which the longitudinal magnetization recovers during each precession period. As pointed out in [5] and as will be shown again here, for most conditions, the equilibrium position is almost along the cycle rotation axis. Thus a good strategy to accelerate the convergence towards equilibrium is to transfer, by the stabilization sequence, the large longitudinal magnetization present at the beginning of the sequence along this cycle rotation axis. It will then begin to decay in magnitude towards its equilibrium value under the influence of the relaxation processes.

2.1. The cycle rotation

The stabilization sequence will rely essentially on the model of the cycle rotation, which is the subject of this section. Let us suppose that the repetition time TR is equal to $2T$. Note that [5,10] use the notation TE in place of T, with $\mathrm{TE} = \mathrm{TR}/2$, but we think it can be misleading in reference to the Fast Spin Echo sequence where TE refers to the time separating the first echo from the flip pulse, which is $2T$. One of the aims of the present article is to make the link between the SSFP sequence and the Fast Spin Echo sequence and actually to consider them as *the same sequence,* only with a different initial condition. Hence the need to alleviate any confusion and to forget altogether the notation TE and use a time unit T defined as half the repetition time in SSFP or as half the echo spacing in FSE. One will consider the cycle starting from the center of one precession interval to the center of the next precession interval, i.e., the cycle would begin and end at the position of echo in an FSE experiment (Fig. 1). One then characterizes the precession by the angle $-\omega$ imposed to a given magnetization by all the longitudinal fields B_0, whether due to gradients or main field inhomogeneity during a lapse of time T (the minus sign in front of ω is to conform to Shinnar–Le Roux algorithm notations and is justified by the fact that the gyromagnetic coefficient γ of the proton is negative). This angle of precession is, as usual, measured in the rotating frame corresponding to the demodulation carrier. The nuta-

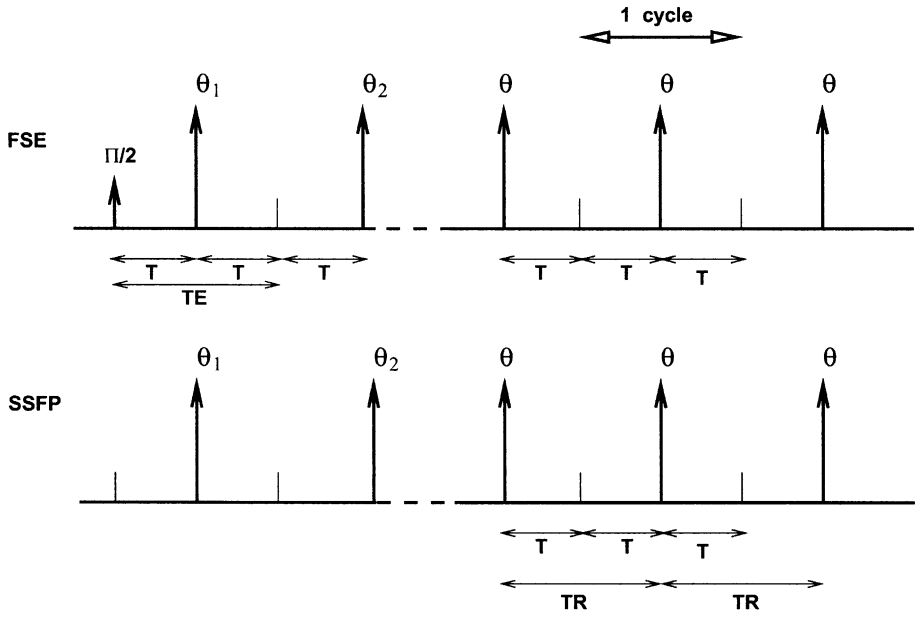

Fig. 1. This article considers a long train of constant RF pulses of nutation θ and separated by $2T$. Rather than considering a cycle from one RF pulse to the next as is generally done in SSFP (bottom figure) we prefer to consider the cycle from the center of the precession period to center of the next precession period, as is natural in Fast Spin Echo (top figure). Indeed SSFP and FSE are the same sequence but with different initial conditions. As in [23] the nutation angle of the first few pulses will be varied; one note θ_1 the first nutation, θ_2 the second ... M_1 is the magnetization at the first measurable echo. The symbols without suffix being reserved for the constant train which follows the stabilization sequence.

tion imposed by the RF pulse is called θ, and is along the axis x of the transverse plane. Neglecting relaxation, one writes the rotation from one echo to the next, first in the form of symbolic rotation operator. One has first a precession $-\omega$, followed by a nutation θ, again followed by a nutation $-\omega$, giving a resulting rotation

$$R = R_z(-\omega)R_x(\theta)R_z(-\omega). \tag{1}$$

In order to derive the numerical expression of this rotation we prefer to use the spinor or SU_2 formalism [11–13], with the same notation as the one used in [14]; in this formalism a precession of angle $-\omega$ is represented by the matrix:

$$Q_z(-\omega) = \begin{bmatrix} \exp(\mathrm{j}\omega/2) & 0 \\ 0 & \exp(-\mathrm{j}\omega/2) \end{bmatrix}, \tag{2}$$

and the nutation of angle θ around x is represented by

$$Q_x(\theta) = \begin{bmatrix} c & -\mathrm{j}s \\ -\mathrm{j}s & c \end{bmatrix}, \tag{3}$$

with $c = \cos(\theta/2)$, $s = \sin(\theta/2)$. It is then a question of elementary calculus to find the SU_2 matrix representing the cycle rotation (1):

$$Q = \begin{bmatrix} c\exp(\mathrm{j}\omega) & -\mathrm{j}s \\ -\mathrm{j}s & c\exp(-\mathrm{j}\omega) \end{bmatrix}. \tag{4}$$

One then uses the fact that one can put any SU_2 matrix in the form

$$Q = \mathcal{C}1 - \mathrm{j}\mathcal{S}\sigma(n_z, n_{xy}), \tag{5}$$

with $\mathcal{C} = \cos(\Omega/2)$ and $\mathcal{S} = \sin(\Omega/2)$, Ω being the angle of the rotation this matrix represents. The axis of the rotation, given by its components n_z along the axis z and n_{xy} its projection in the transverse plane, is found from the matrix σ (vector matrix or density matrix):

$$\sigma = \begin{bmatrix} n_z & n_{xy}^* \\ n_{xy} & -n_z \end{bmatrix}. \tag{6}$$

Isolating the real part of the diagonal elements of (4), one obtains:

$$Q = c\cos(\omega) - \mathrm{j}\begin{bmatrix} -c\sin(\omega) & s \\ s & c\sin(\omega) \end{bmatrix}. \tag{7}$$

And by identification between (7) and (5), (6) one find that the rotation axis is parallel to the vector $\vec{u}$ having component $u_z = c\sin(\omega)$ along z and $u_x = s$ along x. After normalizing this vector, by dividing it by its norm, one obtains:

$$\begin{aligned} n_z &= -c\sin(\omega)/\sqrt{1 - c^2\cos^2(\omega)}, \\ n_x &= s/\sqrt{1 - c^2\cos^2(\omega)}, \\ \Omega &= 2\arccos(c\cos(\omega)). \end{aligned} \tag{8}$$

Note that if the sign of the rotation angle were irrelevant one could prefer $\Omega = 2\arcsin(\sqrt{s^2 + c^2\sin^2(\omega)}) = 2\arcsin|\vec{u}|$. Also one important fact is that $n_y = 0$, i.e., the cycle rotation axis is always in the (x, z) plane. This is what will greatly simplify the analysis and is the reason why it is preferable to consider the cycle from echo to echo.

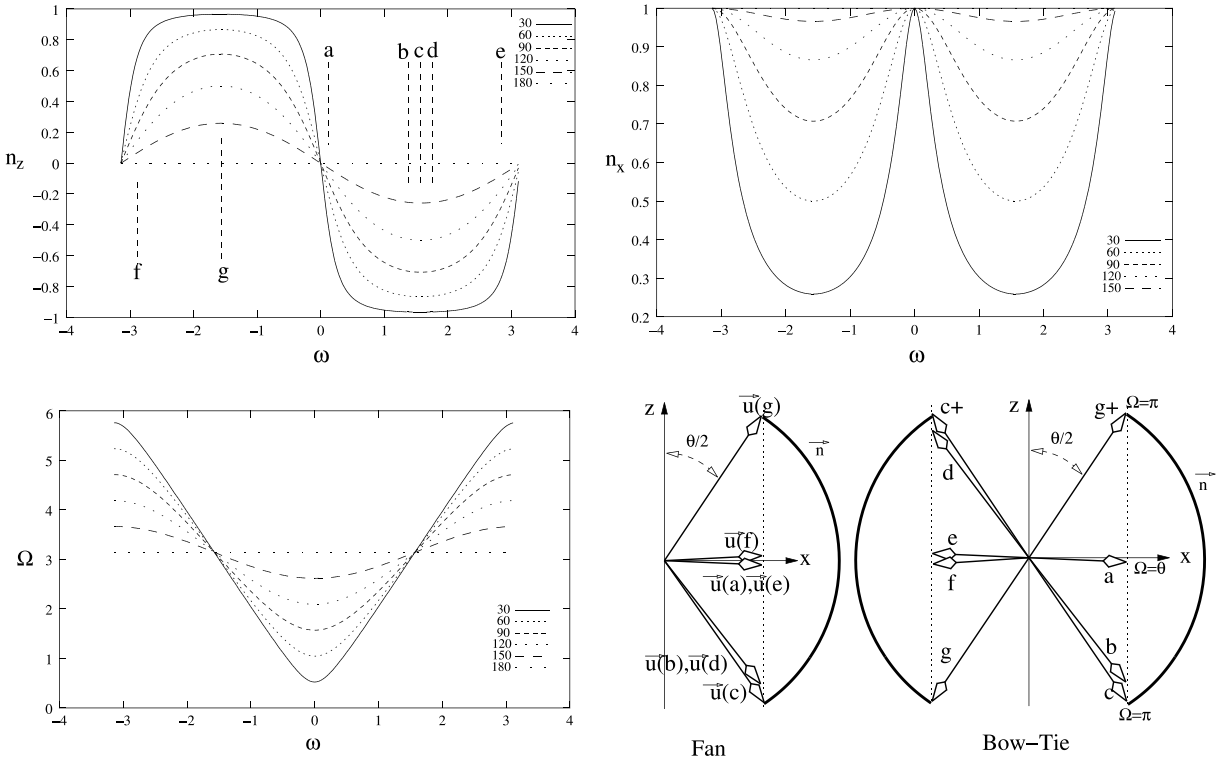

Fig. 2. Top, the z and x components of the normalized rotation axis $\vec{n}$. Bottom left, the rotation angle. Bottom right, the representation of the rotation axis, before normalization, $\vec{u}$ for one nutation angle (here around 70°) and for some precession angles ω as marked by the letters 'a' to 'e' shown on the first graph. The first representation noted fan is conform to the graphs at top. In the representation noted bow-tie, the rotation axis has been toggled to the opposite direction at $\omega = \pm\pi/2$, with a concomitant subtraction of π to the rotation angle. This way the rotation angle is always positive (in fact greater or equal to θ) and inferior to π. The rotation axis mimics somewhat the effective field for two constant, but opposite, RF excitations centered at $\omega = 0$ and $\omega = \pi$.

Fig. 2 summarizes these equations in graphic form, for different nutation angles. Some key points are: for $\omega = 0$ the axis of rotation is along x and the angle of nutation is θ, for $\omega = \pi$ the nutation angle is $-\theta$; for $\omega = \pi/2$ or $\omega = -\pi/2$ the rotation angle is $\Omega = \pi$ along an axis which is tilted away from, respectively, $-z$ or z by an angle $\theta/2$. The same axis of the rotation is obtained twice for ω and $\pi - \omega$. This is related to the fact that one has considered the rotation angle Ω to be always positive, actually varying between θ and $2\pi - \theta$, and a 'mean value' around π. This representation has the advantage to furnish continuous waveforms for n_z, n_x, and Ω. It gives a graphical representation of the rotation axis in a 'fan' form as in Fig. 2. Another approach is to constrain the rotation angle between $-\pi$ and $+\pi$, and changing abruptly the rotation axis to the opposite direction at $\omega = \pi/2$ and $\omega = -\pi/2$ (where the rotation angle attains $\pm\pi$). This can be called the 'bow-tie' representation.

Without relaxation, the dynamic of the system is easily studied by decomposing any magnetization $\vec{M}_k$ at echo k along the axis of the rotation $\vec{n}$ (this component will stay constant) and the perpendicular plane spanned by the original axis of the rotating frame $\vec{y}$ and a third vector, called $\vec{v}$, having components $(-n_z, 0, n_y)$ in the $\vec{x}, \vec{y}, \vec{z}$ frame. The magnetization fraction contained in this plane $(\vec{y}, \vec{v})$ undergoes a rotation by an angle Ω between each echo. One will refer to this component of magnetization by the term 'perpendicular' component, while one will call the component along $\vec{n}$ the 'parallel' component, reserving the usual terms longitudinal and transverse to the decomposition along the axis $\vec{z}$ and the plane $\vec{x}, \vec{y}$ of the original frame. We will call the frame defined by the vectors $\vec{n}, \vec{y}, \vec{v}$ the cycle rotation frame.

2.2. Relaxation effects

The evolution equation without relaxation turns out to be the backbone permitting an easy study of the relaxation in SSFP or FSE. During the precession periods the relaxations processes tends to diminish the two transverse components x, y with a time constant $T_2 = 1/\omega_2$ and the z component with a time constant $T_1 = 1/\omega_2$. That is to say, defining $e_1 = \exp(-\omega_1 T)$, $e_2 = \exp(-\omega_2 T)$, and the diagonal matrix

$$E = \begin{bmatrix} e_2 & & \\ & e_2 & \\ & & e_1 \end{bmatrix},$$

the transfer from echo $k-1$ to echo k becomes:

$$M_k = AM_{k-1} = (ERE)M_{k-1}. \quad (9)$$

When the transverse and longitudinal relaxations are equal $e_1 = e_2 = e$ there is no change in the eigenvectors of the matrix A and the eigenvalues are multiplied by e. The difficulty arises when $\omega_1 \neq \omega_2$. It is shown in Appendix A that under the condition that $\omega_2 T$ is not too small and at least for a range of precession angle ω excluding a small portion around $\omega = 0$ and $\omega = \pi$, the eigenvectors are not very different from the non-relaxing case (this was also noted in [5]). In addition, this appendix gives as an approximation of the relaxation rate of the component parallel to the rotation axis $\overrightarrow{n}$:

$$\omega_{\|} = n_x^2\omega_2 + n_z^2\omega_1. \quad (10)$$

One can use the following mnemonic: because $n_x^2 + n_z^2 = 1$, one can consider n_x^2 as being the proportion of time the magnetization spends along $\overrightarrow{x}$, relaxing at the rate ω_1, while n_z^2 is the proportion of time the magnetization is along $\overrightarrow{z}$ relaxing at the rate ω_1. The notation $\omega_{\|}$ could be replaced by the notation $\omega_{1\rho} = 1/T_{1\rho}$ to relate it to the classical continuous relaxation along the effective RF field [15], which has similar expression to Eq. (10).

The component in the $(\overrightarrow{y}, \overrightarrow{v})$ plane relaxes at the rate:

$$\omega_{\perp} = \frac{\omega_2}{2} + \frac{n_x^2\omega_1 + n_z^2\omega_2}{2}. \quad (11)$$

Again one can consider the following mnemonic: the perpendicular magnetization spends one half of the time along $\overrightarrow{y}$, and one half of the time along $\overrightarrow{v}$, and the time along $\overrightarrow{v}$ is distributed in proportion n_x^2 and n_z^2 along $\overrightarrow{z}$ and $\overrightarrow{x}$.

Taking now into account the T_1 recovery during the precession periods, a constant vector parallel to $\overrightarrow{z}$ is added at the right member of the recursion (9) (see Appendix B). But again, projecting the magnetization in the cycle rotation frame, and under broad conditions, one arrives at the fact that the perpendicular component of the dynamic equilibrium is negligible, whereas the parallel component has an algebraic length, noted $\overline{m}$, along $\overrightarrow{n}$ which is

$$\overline{m} = n_z\frac{\omega_1}{\omega_{\|}} = n_z\frac{\omega_1}{n_x^2\omega_2 + n_z^2\omega_1}. \quad (12)$$

Again this can be compared with the classical continuous expression in [15]. And the x, z components of the equilibrium magnetization $\overline{m}\overrightarrow{n}$ are obtained by scaling the components of the rotation axis n_x, n_z as given by Eq. (8) by $\overline{m}$ in Eq. (12). Fig. 3 shows the result of this operation for $T = 5\,\text{ms}$, $T_1 = 400\,\text{ms}$, $T_2 = 100\,\text{ms}$ (these values are chosen to be able to compare with [5], although typically the value of T should rather be in the 1.5 ms range). The discrepancy between this result and the full solution [9] could not be seen on this figure. Even with $T_1 = 700\,\text{ms}$ and $T_2 = 40\,\text{ms}$ (heart muscle) the discrepancy between the proposed simplified Eqs. (8) and (12) and the full solution is only sensitive at low nutation angle (below 30°) and only in a very limited range of ω around 0 and π.

2.3. Actively reducing the perpendicular component

Although interesting in its own sake the study of the relaxation is not that important for the stabilization of signal. The most important result from the previous paragraph is that the axis of the rotation (or damped rotation) is not changed significantly: it is shown here that a good strategy is to put the magnetization rapidly along that axis, whatever the relaxation effects, and then let it relax at its own pace.

In standard, dispersed or crushed, sequences like FSE or SSFP one measures the sum of all transverse magnetizations for all the precession angles ω. It is known, at least in the case of FSE, that even without relaxation the signal is stabilized quite quickly. This is due to the dispersion of rotation angles Ω with which the

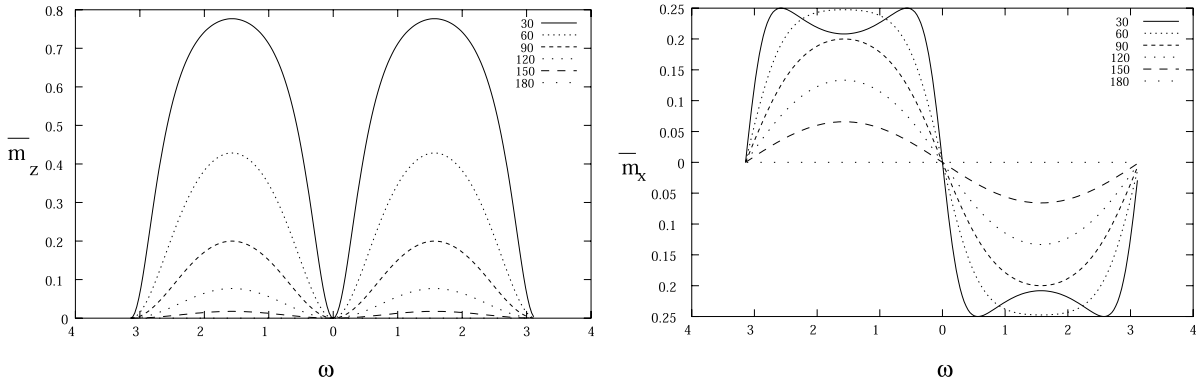

Fig. 3. Longitudinal and transverse dynamic equilibrium magnetization, at echo time of a refocused SSFP, under relaxation with $T_1 = 400\,\text{ms}$, $T_2 = 100\,\text{ms}$, $T = 5\,\text{ms}$ (TR = 10 ms), for different nutation angles. This curves where obtained by simulating the Bloch equations but there is no visible difference between this curves and the one obtained by using the much simpler model given by Eqs. (8) and (12).

component perpendicular to the rotation axis oscillates. Although each individual perpendicular component can be very large (in some cases equal to the original magnetization) they tend after a while to disperse and the global magnetization in one pixel becomes the sum of only the parallel components. It is as if the dispersion had produced a projection of the original magnetization M_0 on the local axis of the rotation, leaving only the parallel component $m_{\|}$ (of length n_z) of the original magnetization M_0, see Fig. 4. Incidentally this is how one can demonstrate that the signal of FSE is proportional to $\sin(\theta/2)$, a result which, to the knowledge of the author, has never been demonstrated (see Appendix B). This signal stabilization by projection and dispersion seems to be the phenomenon used recursively in [16]. In summary the phase dispersion plays a role very similar to the one the relaxation plays, even when the latter one is not present or not significant, and this phase dispersion stabilizes naturally the received signal. One can do the same analysis for the SSFP sequence (Fig. 5). Note that according to Eq. (12) the relaxed equilibrium value along the rotation axis, $\overline{m}$, is in fact $m_{\|} \times (\omega_1/\omega_{\|})$ and is equal to the dispersed equilibrium value if $T_1 = T_2$, but is generally smaller. Now this beneficial action of dispersion, and actually the notion of dispersed equilibrium, vanishes entirely in the case of a refocused sequence. If the sequence is fully refocused there is only one definite precession angle in each pixel and there is a single oscillating signal, with a well defined frequency Ω, generated by the perpendicular component. This signal can be higher than the constant signal, and will not diminish otherwise than by relaxation if nothing is changed in the excitation sequence. The aim of the stabilization period is to reduce as quickly and as thoroughly as possible the perpendicular component of this magnetization. This action has to be fast, lasting only some echo spaces, and cannot rely on any relaxation process; hence this operation is necessarily a rotation for which at any interval k, $|M_k| = |M_0|$. The only way to eliminate the perpendicular component of M_k is to drive it towards the local rotation axis $\overrightarrow{n}$, but this time keeping, almost by obligation, its full magnitude. Thus at the end of the preparation period, composed of p RF intervals, the magnetization M_p must be $M_p = \pm|M_0|\overrightarrow{n}$. In the case of the SSFP sequence (see Fig. 5), because the original magnetization is along $\overrightarrow{z}$ and the ultimate position after the relaxation process is also with z positive (see previous paragraph), the sign in the last equation is logically $\mathrm{sign}(n_z)$. The target magnetization at the end of the preparation period is thus $M_p = \mathrm{sign}(n_z) \times \overrightarrow{n}$. The loci

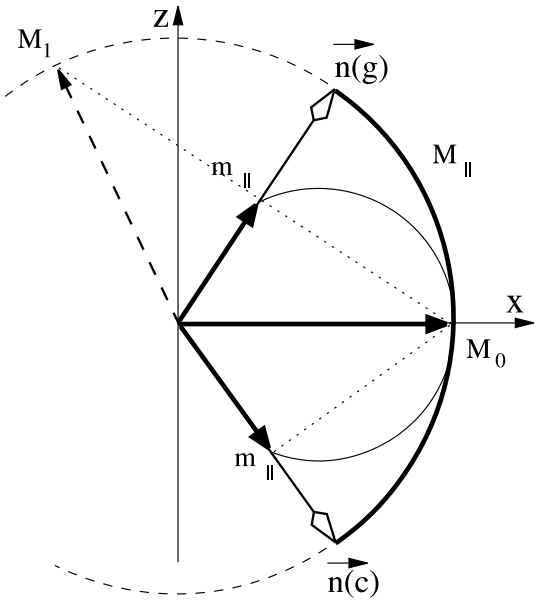

Fig. 4. Signal stabilization by phase dispersion in a non-refocused FSE sequence the labels 'c' and 'g' in $\overrightarrow{n}(c)$ and $\overrightarrow{n}(g)$ refer to precession angle values, as in the series 'a' to 'g' depicted in Fig. 2). The original magnetization is along the x axis. Consider a precession angle of $\omega = -\pi/2$ with a rotation axis $\overrightarrow{n}(g)$: the original magnetization is broken up into a components parallel and perpendicular to the rotation axis. The perpendicular part enter an oscillatory movement with a rotation angle Ω, which in the considered case is π, putting the magnetization at M_1 at time of echo 1. But this rotation angle Ω is spread in the range $-\pi$, π and the oscillatory components experience a phase dispersion which rapidly cancel out the overall signal they generate, leaving only, in the case of crushed FSE, the constant signal generated by the parallel components. The extremities of these components when ω varies in the $\pm\pi$ range is shown by the thin solid arc of circle $M_{\|}M_0M_{\|}$. In case of a refocused FSE there would be only one definite, but uncontrolled, value of ω in one pixel and the only way to guarantee the absence of oscillatory signal is to actively drive the original magnetization to a position parallel to the rotation axis (positions shown by the wide arc of circle $n(g)M_0n(c)$).

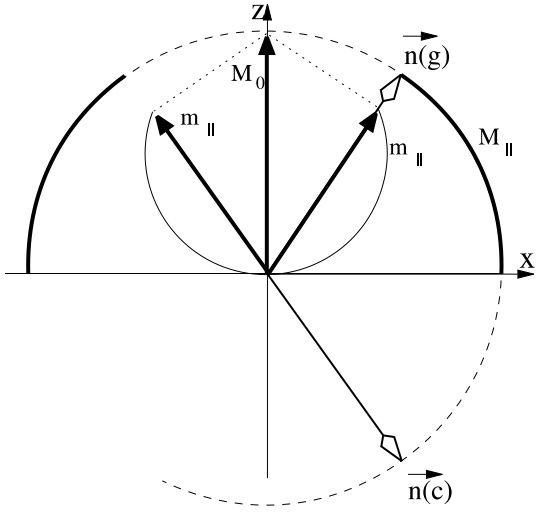

Fig. 5. Analysis similar to Fig. 4 can be applied to SSFP the labels 'c' and 'g' in $\overrightarrow{n}(c)$ and $\overrightarrow{n}(g)$ refer to precession angle values, as in the series 'a' to 'g' depicted in Fig. 2). This time the original magnetization is along z. $\mathrm{m}_{\|}$ is the projection of the original magnetization onto the rotation axis and is also the point towards which the magnetization $\overline{m}$ will relaxed if $T_1 = T_2$. For reducing rapidly the oscillation one must put the magnetization, still with its full magnitude along the rotation axis, i.e., along the bold arcs of circle noted $M_{\|}$.

of this target position for different precession angles ω are shown in Fig. 5 by the two bold arcs of circle (representing the superior half of a bow-tie). And we highlight this stabilized magnetization $M_{\|}$ to distinguish it from the smaller dispersed $m_{\|}$ equilibrium and from the still smaller relaxed equilibrium $\overline{m}$. If the corresponding components along x and z were drawn they would have the general form of the dispersed or relaxed equilibrium as shown in Fig. 3 but it would present a strong discontinuity at $\omega = 0$ and $\omega = \pi$; this discontinuity is of course impossible to realize, at least in a finite preparation time, and there will be some range of ω around 0 and π where it will be impossible to eliminate the perpendicular component. To reduce the corresponding signal oscillation one will need a selective saturation prior to the stabilization sequence, with the usage of some crushing gradients, as suggested in [5], eliminating altogether any signal, useful or parasitic, coming from the $\omega = 0$, $\omega = \pi$ regions. This pre-saturation will be not considered in the present article; but we will try to reduce as much as possible the extent of precession frequencies where the perpendicular component cannot be eliminated, and outside this band of frequencies we will try to reduce as much as possible the residue of perpendicular magnetization. In this stabilized region, the magnetization will then be almost aligned with $\overline{m}\,\overrightarrow{n}$ but with a larger magnitude equal to the original M_0 after the preparation. It will, at that time, start a relaxation process with the relaxation rate $\omega_{\|}$ towards $\overline{m}\,\overrightarrow{n}$, generating perhaps some blurring, as in any fast sequence, but no artifact.

3. Stabilization of SSFP

As outlined in the introduction we intend to use for stabilization of the refocused SSFP a generalization of the linear ramping proposed by [8]. A better justification of the results obtained by a linear ramping is given here. This new justification relies on a change of frame, similar to the one used in adiabatic RF excitations.

3.1. Slowly varying cycle rotation frame

In this section the nutation angle θ_k of each RF pulses will be varied. This results in a rotation from echo number $k-1$ to echo number k, R_k, characterized by variable rotation angle Ω_k and axis $\overrightarrow{n}_k$. These values are calculated in an analog manner to the constant nutation case used in Eq. (8) but with c and s replaced by $c_k = \cos(\theta_k/2)$ and $s_k = \sin(\theta_k/2)$. One will note ϕ_k the angle between the axis $\overrightarrow{z}$ and the rotation axis $\overrightarrow{n}_k$. One reserves the non-indexed symbols Ω and ϕ to the parameters of the constant echo-to-echo rotation induced by the train of constant nutation θ which follows the stabilization period.

The echo number 0 is by convention the echo before the first RF pulse, which is the time of the end of the flip pulses in an FSE experiment. The first RF pulse is θ_1, and the first echo to echo rotation (from echo 0 to echo 1) is characterized by $\Omega_1, \overrightarrow{n}_1$ (see Fig. 1). The magnetization at the first measured echo is noted $\overrightarrow{M}_1$.

Let us define a varying cycle rotation frame whose $\overrightarrow{z}'$ axis stays aligned with the rotation axis $\overrightarrow{n}_k$(Fig. 6). The rotation axis stays in the (x,y) plane, and the other vectors composing the frame can be taken as $\overrightarrow{x}' = \overrightarrow{v}_k$, perpendicular to $\overrightarrow{n}_k$ in the (x,y) plane, and $\overrightarrow{y}' = \overrightarrow{y}$. One supposes that this frame is kept as the reference from just after the time of echo $k-1$, until the time of echo k when the magnetization $\overrightarrow{M}_k$ is measured; then, instantaneously, one switches to the the next frame relative to the cycle rotation from echo k to echo $k+1$. That means that just after echo $k-1$, one has to add a corrective rotation along the $\overrightarrow{y}$ axis with an angle

$$\delta_k = \phi_k - \phi_{k-1}. \tag{13}$$

This correction is to be applied for $k = 1\ldots$, and with the special value $\phi_0 = 0$, as one takes by convention the original rotation axis aligned with $\overrightarrow{z}$ at echo 0. One assigns the index p to the first RF pulse having a nutation angle equal to the target value θ, $\theta_p = \theta$; all posterior RF pulses will have that nutation angle θ. Hence

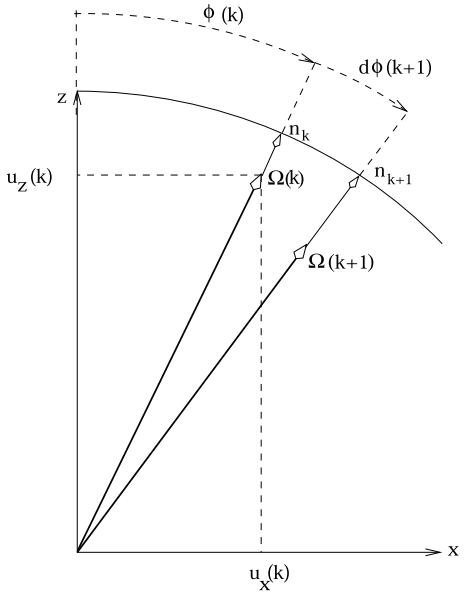

Fig. 6. When the nutation angle θ_k varies, the 'cycle' rotation, from echo $k-1$ to echo k varies according to Eq. (8). The angle ϕ_k between the rotation axis $\overrightarrow{n}_k$ and the axis $\overrightarrow{z}$ varies, and also the rotation angle Ω_k. In a new frame whose $\overrightarrow{z}$ axis would stay aligned with $\overrightarrow{n_k}$ for all k, a rotation with an angle $\mathrm{d}\phi_k = \phi_{k+1} - \phi_k$ would have to be added along $\overrightarrow{y}$. If this corrective term is small enough the rotation in the new frame is a pure precession and the angle between the magnetization and the axis $\overrightarrow{n_k}$ would stay constant (adiabatic-like condition). This condition is not easy to realize, but a more acceptable hypothesis is to suppose that the corrective nutation $\mathrm{d}\phi_k$ is small enough to permit the classical linear approximation analysis of RF excitation in this new frame.

from $k = p + 1$, onwards the correction rotation along $\overrightarrow{y}$ is nulled $\delta_k = 0$, $k > p$. In the cycle rotation frame, the following sequence of rotations and measurement (noted S_k for 'sampling') takes place: $R_y(\delta_1), R_{z'}(\Omega_1), S_1, R_y(\delta_2), \ldots, S_{p-1}, R_y(\delta_p), R_{z'}(\Omega_p), S_p$, followed by $R_{z'}(\Omega), S_{p+1}, R_z(\Omega) \ldots$.

If one supposes that the rotation along y is negligible in regard to the rotation along $\overrightarrow{z}'$,

$$\delta_k < \Omega_k / k_A, \tag{14}$$

with k_A a coefficient which must be sufficiently large (for instance greater than 10), the axis of the combined rotation $R_y(\delta_k)R_{z'}(\Omega_k)$ is almost collinear to $\overrightarrow{z}'$ and one obtains easily the result that the magnetization stays almost aligned with the axis of the cycle rotation if it were aligned with it at the time origin (echo zero). The condition (14) is similar to the definition of adiabatic condition in MR excitation [11,17,18]. Unhappily, it appears that this adiabaticity-like condition is too restrictive. Defining the sensitivity

$$w_k = \frac{\partial \phi_k}{\partial \theta}, \tag{15}$$

and approximating $\delta_k = \phi_k - \phi_{k-1}$ by $\delta_k = w_k(\theta_k - \theta_{k-1})$, the condition (14) is realized if the rate of variation of the nutation angle θ is small enough,

$$\theta_k - \theta_{k-1} < \frac{1}{k_A}\frac{\Omega_k}{w_k}. \tag{16}$$

Unhappily by plotting $\Omega(\theta, \omega)$, according to Eq. (8), and $w(\theta, \omega)$, which is found after some manipulation to be equal to $\sin(\omega)/(2\sin^2(\Omega/2))$, on Fig. 7, one realizes that the rate of variation of θ should be very small particularly for precession angles ω close to zero (or π).

The next level of approximation which is far less restrictive is to admit that the corrective rotations $R_y(\delta_k)$ are small enough for the parallel magnetization component along $\overrightarrow{z}' = \overrightarrow{n}_k$ to stay constant and $\simeq 1$, but without supposing that the perpendicular component of $\overrightarrow{M}_k$, noted $\overrightarrow{\varepsilon}_k$ in the following, *is null at all time*; this is typically the kind of approximation (first order approximation) one does for calculating the transverse magnetization under the influence of a small (and of short duration) RF field using the Bloch equations. Here the RF field role is played by δ_k, and in the cycle rotation frame the first order approximation of the perpendicular component can be written

$$\overrightarrow{\varepsilon}_k = R_{z'}(\Omega_k)(\overrightarrow{\varepsilon}_{k-1} + \overrightarrow{v}\delta_k). \tag{17}$$

If ε_k is the complex value such that

$$\overrightarrow{\varepsilon}_k = \mathrm{Re}(\varepsilon_k)\overrightarrow{v} + \mathrm{Im}(\varepsilon_k)\overrightarrow{y}. \tag{18}$$

Eq. (17) can be more compactly written as a first order equation in the complex variable ε

$$\varepsilon_k = \exp(\mathrm{j}\Omega_k)(\varepsilon_{k-1} + \delta_k), \tag{19}$$

which in turn, after defining

$$\varphi_k = \sum_{i=1}^{k} \Omega_k, \tag{20}$$

and $\varepsilon_k = \epsilon_k \exp(\mathrm{j}\varphi_k)$, becomes

$$\epsilon_k = \epsilon_{k-1} + \mathrm{e}^{(\mathrm{j}\varphi_k)}\delta_k.$$

Noting that $\varepsilon_0 = \epsilon_0 = 0$, one obtains finally

$$\epsilon_p = \sum_{k=1}^{p} \delta_k \exp(\mathrm{j}\varphi_k). \tag{21}$$

If Ω_k were constant and equal for instance to the value $\widehat{\Omega}$, one would have $\varphi_k = \widehat{\Omega}k$ and the above equation would define the perpendicular magnetization at the end of the preparation period as the Discrete Fourier Transform of the sequence δ_k at the reduced radial frequency $-\widehat{\Omega}$. The left part of Fig. 7 shows that this is indeed the case at least for small θ, where we have $\widehat{\Omega} \simeq 2\omega$. Hence, at least for the beginning of a ramp up,

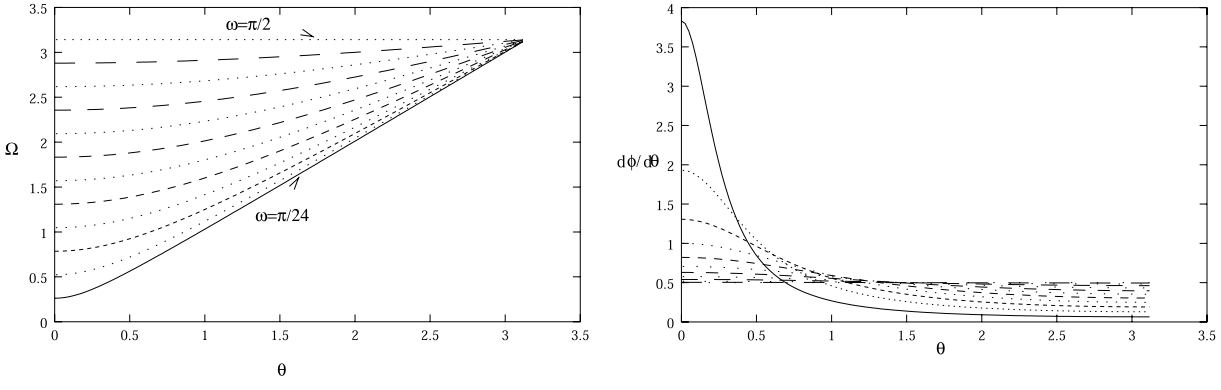

Fig. 7. Left the rotation axis in function of the nutation angle is shown for different precession angles. It is large and close to π when the precession angle is around $\pi/2$. Also Ω is quasi constant and equal to 2ω, for small θ. The sensitivity $w = \partial\phi/\partial\theta$ is shown on the right. The very high sensitivity of ϕ in regards of θ, when ω and θ are small, impede the adiabatic-like, zero order, approximation to be valid except for very slow ramp up and/or for a reduced range of precession angle ω. For the, then necessary, first order analysis it is interesting to note that the sensitivity $\partial\phi/\partial\theta$ around $\theta = 0$ is relatively constant and equal to $1/(2\sin(\omega))$.

ϵ_k, at the precession angle ω, is the Discrete Fourier Transform of δ_k the first difference of the tilt angle ϕ of the cycle rotation axis, at the reduced radial frequency -2ω. Also the right part of the figure shows that at small nutation angle again the sensitivity w is quasi constant with the value $w = 1/(2\sin\omega)$. Hence, noting the rate of variation of the nutation angle by

$$\Delta_k = \theta_k - \theta_{k-1}, \tag{22}$$

(with by convention $\theta_0 = 0$ and hence $\Delta_1 = \theta_1$), we obtain

$$\epsilon_p(\omega) = \frac{1}{2\sin(\omega)} \sum_{k=1}^{p} \Delta_k \exp(\mathrm{j}2\omega k). \tag{23}$$

We thus can express, for any precession angle ω, the perpendicular magnetization in terms of the discrete Fourier transform of the first difference of the nutation angle sequence θ_k.

Actually as $1/\sin(\omega)$ is proportional to the Fourier transform of a summation, the perpendicular magnetization can be expressed directly as a function of the Fourier transform of the sequence of nutation angle θ_k but including the $p+1$th pulse θ_{p+1} which is equal to the pth pulse θ_p. The obtained expression is in fact more complicated than (23). Conversely because one has, around $\omega = \pm\pi/2$, $\sin(\omega) = 1$ we can simplify (23) into

$$\epsilon_p(\omega) = \frac{1}{2} \sum_{k=1}^{p} \Delta_k \exp(\mathrm{j}2\omega k), \tag{24}$$

making the perpendicular magnetization directly equal (with a constant coefficient 0.5) to the Fourier transform of the rate of change of nutation. For precession angles approaching the critical precession angle 0 and π both approximations (23), (24) diverge from the reality but in the same amount, the first one (23) by excess in magnitude, the other one (24) by default. For simplicity we will adopt, in the following, the lighter model (24).

This first order approximation in the cycle rotation frame probably justifies the linear hypothesis taken in [8]. In the frequency regions around $\omega = 0$ or $\omega = \pi$, the Fourier transform result (23) is not valid, and only simulation results will be useful.

3.2. Simulation results of a linear ramp

Fig. 8 shows with a linear scale and a logarithmic scale (in decibels) the magnitude of the perpendicular magnetization, and, for comparison, the results of the linear approximation (24), when the nutation angle is a linear ramp of 8 pulses $\theta_1 = 1/8, \ldots, \theta_7 = 7/8, \theta_8 = 1$, for a stabilized $\theta = 1$ rad. Note that as the last stabilization pulse is already equal to θ, the echo signal preceding it (of index 7) should be considered as already stabilized; in the following, a preparation made of p RF pulses describes a preparation sequence where the last pulse has a nutation angle equal to the target rotation θ, and the echo preceding it (with index $p-1$) presents already the minimum error ϵ; hence, there is actually only $p-2$ echo measures to disregard in this case.

To simulate the true perpendicular magnetization at echo p, one calculates this magnetization for 512 equidistant values of ω ranging from $-\pi$ to π, by performing the product of 3×3 rotation matrices similarly to (9) (Bloch equations). The original magnetization at echo 0 has a length one and is along the $\vec{z}$ axis. The magnetization at echo $p = 8$ is projected into the cycle rotation frame $\vec{v}, \vec{y}, \vec{n}$ corresponding to $\theta = 1$ and that for each ω, to obtain $\epsilon(\omega)$. For comparison the perpendicular magnetization according to the approximate theory (24) is calculated.

As can be appreciated from Fig. 8 the linear theory is validated in a large part of the attenuated band of the sinc response. One note that in this region both the approximation and the reality presents lobes with an amplitude decreasing in $1/\omega$. When one increases the length p of the ramp there is a contraction of all the lobes, and a proportional addition of secondary lobes; but the maximum ripples of the secondary lobes remain somewhat constant and at a given precession angle ω in the stop band the ripple decrease very slowly according

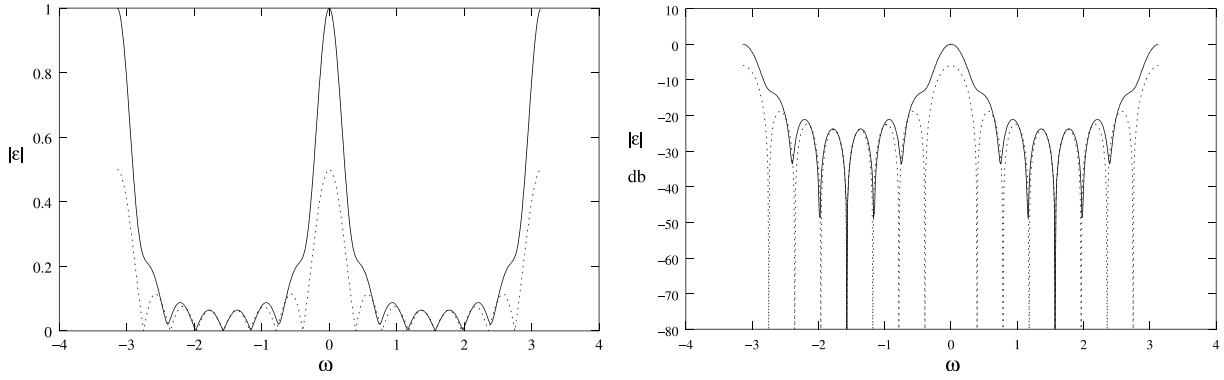

Fig. 8. The absolute value of the perpendicular component at the end of the stabilization period, when using a linear ramp of length $p = 8$, compared with the linear approximation given by Eq. (24) which is valid around $\omega = \pm\pi/2$. Linear scale at left and logarithmic scale at right.

to a law in the order of $1/p$ when one increases the duration p of the preparation. It is known in Finite Impulse Response filter design that by accepting a larger transition bandwidth one can have ripples amplitude which decrease exponentially with p when using good apodization window.

3.3. More flexible window

The Kaiser Bessel window [19] is the most flexible window and gives result very close to the min–max optimum which would be obtained by the Dolph–Chebishev window [20] which is more difficult to program. It is governed by a parameter β which, in addition to the length of the window, allows a compromise between the width of the transition band and the ripple in the stop band; For $\beta = 0$ one obtains the boxcar window corresponding to the linear ramp as tested in the previous section. This Kaiser window will thus permit to generalize the results just obtained by a linear ramp.

To design a Kaiser Bessel window, one first defines a reduced time

$$\tau(k) = ak + b$$

k being in the present case the RF pulse index $1, \ldots, p$. a and b are adapted such that for the first pulse, $k = 1$, one has $\tau = -1$ and for the last pulse, $k = p$, $\tau = +1$. Then the Kaiser window, to which one will identify the first order difference of the nutation angle (22), is in the form

$$\Delta(k) = GI_0(\beta\sqrt{1-\tau^2(k)}) \tag{25}$$

G being a static gain that one has to adapt such that, after summation, the nutation of the RF pulse p is

$$\theta(p) = \sum_{k=1}^{p} \Delta(k) = \theta. \tag{26}$$

In (25), I_0 is the modified Bessel function of order 0 which can be computed by series expansion [19] if necessary. As said, the parameter β allows compromise between a narrow main lobe but large ripple as obtained for $\beta = 0$ (the boxcar window), or a wide main lobe and small stop band ripple. For $\beta = 5$ the first ripple is 1.2% of the main lobe amplitude but at the price of a transition bandwidth which is almost doubled. Also at these large values of β the first pulse nutation $\theta(1) = \Delta(1)$ is very small and the non-linearity of the exciter probably does not permit to play faithfully all the pulses of the preparation. That is why Fig. 9 compares the original 8 pulses linear ramp to $\theta = 1$ rad, with a 8 pulses Kaiser ramp with a β of only 3; for this value of β, the main lobe of the magnetization response is almost identical for the two preparations, but when the first ripple of the linear (theoretical) preparation attains 10%, the first lobe of the Kaiser preparation is only 2%. The simulation result of Fig. 9 which takes into account the non-linearity of the Bloch equation, justifies the approach taken.

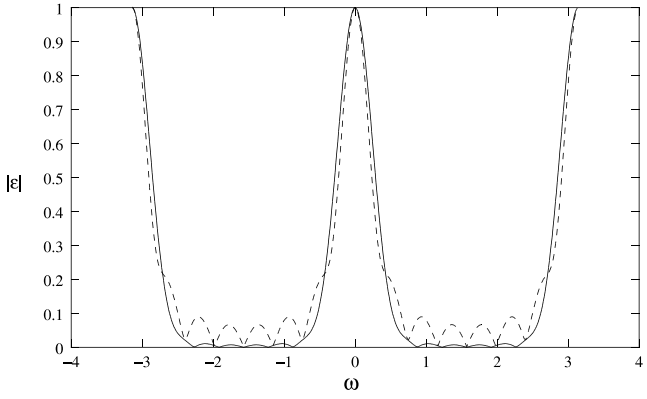

Fig. 9. Responses in the cycle rotation frame for preparations of length 8 (six echoes to be discarded). One, in dotted line, is the linear ramp already shown in Fig. 8, the other one, in solid line, is a Kaiser window with $\beta = 3$. Although the center of main lobe is slightly wider for the the $\beta = 3$ window, the non-linearity in the first secondary lobe make this last window actually better, and in the stop band where the linear approximation becomes valid, the attenuation is much better.

3.4. From the cycle rotation frame back to the rotating frame

In order to evaluate the true magnetization after $p-1$ pulses we had to rely on the Bloch equations which are simply written in the original rotating frame x, y, z and then decompose this magnetization $\overrightarrow{M}_p$ in the frame $(\overrightarrow{n}, \overrightarrow{v}, \overrightarrow{y})$ of the echo to echo cycle rotation R. We obtain along the rotation axis $\overrightarrow{n}$ a component $M_{\|}$, and along the perpendicular plane $(\overrightarrow{y}, \overrightarrow{v})$ a component that we have noted with a complex number ε_p. The parallel component will stay constant and gives a constant transverse magnetization, or signal

$$M_{xy}(\omega) = M_{\|}(\omega)n_x(\omega). \tag{27}$$

For $k > p$ one has for the perpendicular component of magnetization (19) $\varepsilon_k = \varepsilon_p \exp(\mathrm{j}\Omega(k-p))$, but this corresponds to a vector which is in the $(\overrightarrow{v}, \overrightarrow{y})$ plane (18), and after projecting this vector in the $(\overrightarrow{x}, \overrightarrow{y})$ plane one obtain

$$M_{xy}(\omega, k) = \varepsilon_p \exp(\mathrm{j}\Omega(k-p)) \times (n_z+1)/2 + \overline{\varepsilon_p} \exp(-\mathrm{j}(\Omega(k-p)) \times (n_z-1)/2. \tag{28}$$

Hence one has two artifacts positioned symmetrically around the object, at position corresponding to $\pm\Omega$ along the encoding direction, with respective amplitude $|\varepsilon_p||(n_z+1)/2|$ and $|\varepsilon_p||(n_z-1)/2|$.

4. Experimental results

When it was said in Section 2.3 that the dispersion effect was not available anymore in refocused sequence, that was counting without the unintended precession and nutation angles dispersions which tend to render the

artifacts less visible than predicted by the theory. And indeed Epstein et al. [21] suggest to reintroduce some dephasing in order to regain part of the natural stabilization in the True FISP sequence. It is not guaranteed though that this dispersion introduced artificially will not be cancelled by a local gradient, making the artifacts as strong as the ones shown here, where, on the contrary, all precautions have been taken in order to minimize the dispersion effects.

Fig. 10 was obtained by acquiring 31 images of a tap water sphere (a ping-pong ball actually). The acquisition gave 128×128 pixels, interpolated to 256×256, in a square field of view of 28 cm. The object is a sphere in order to reduce as much as possible any resonant frequency gradients, and hence precession angle ω gradients, in the object. The tap water rules out any relaxation during the signal acquisition, but imposed a long recovery period (6 s). The slice thickness was large enough to guarantee that the object was contained entirely in the flat portion of the RF pulse profile and thus only one definitive nutation angle was to be considered: 60° in the following experiments. Each images was acquired with a different central frequency. This variable central frequency was such that the precession angle ω spanned an interval 0 to π when the acquisition number varied from 0 to 31 (actually the central frequency was kept constant, but a linear phase modulation was applied in function of the RF pulse index, and also the receiving period index, to simulate this variable ω). The images were cropped to their central portion along the read axis and collated. The central line of spheres represents then the reconstructed object and the two lateral lines are the artifact with a position which should be along a curve $\Omega(\omega)$, with $\Omega = \pm\pi$ corresponding to the borders of the field of view along the phase encoding direction and $\Omega = 0$ to the central position. One verifies that the curve $\Omega(\omega)$ which is overlaid fits rather nicely the central positions of the artifacts. In the experiment of Fig. 10 no ramping or preparation of any kind was applied, and as expected in this case the artifacts are in the same order of magnitude as the object. For other experiments a linear or Kaiser ramp up was used, in which case the artifacts are much lower in the attenuated region (although still of high amplitude around $\omega = 0$ and $\omega = \pi$). For that reason the images are not shown in fear of the difficulty in rendering the high dynamic of grey level obtained. But for each acquisition a constant circular region of interest was positioned (manually) around the reconstructed object and around the two artifacts; the average grey level was recorded, and these values were plotted and compared to the theoretical curves. Two unknown parameters, the receiver gain, and the slight resonant frequency offset, were chosen appropriately for each run of experiment (by run, it is meant all experiments done the same day, after one unique RF, and central frequency calibration) for scaling and shifting the theoretical curves which were otherwise obtained by the simulation of the first p rotations and the use of the projection equations (27) and (28). Fig. 11 shows the results of two such experiments,

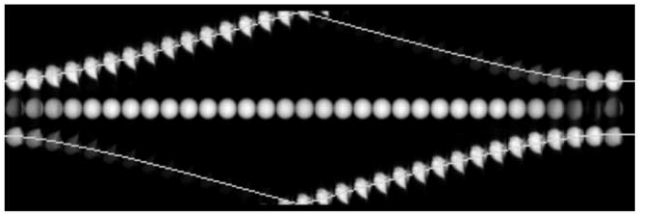

Fig. 10. This figure was obtained by collating, from left to right, the central portion (along the read direction) of 32 different acquisitions of a sphere of distilled water. The encoding direction is from top to bottom. The nominal setting $\omega = \pi/2$ is around the center of the collated image (and correspond to a change of sign of the RF every other pulse), $\omega = 0$ and $\omega = \pi$ are nearby the right and left borders. The theoretical position of the artifacts at $\pm\Omega(\omega)$ (Eq. (8)) has been overlaid. No ramping was used and at least one of the artifacts amplitude is in the same order of magnitude than the object.

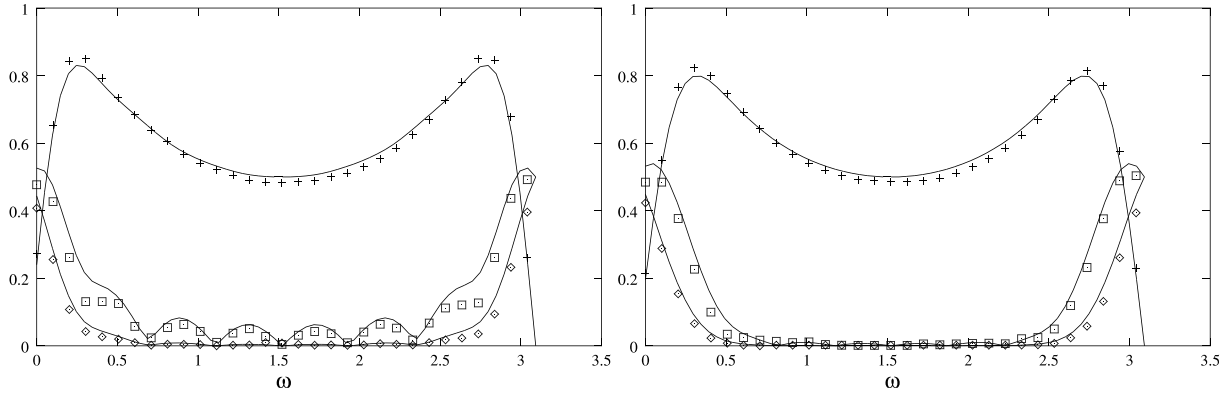

Fig. 11. The experimental values in this figure, represented by crosses, diamonds and squares, have been obtained from two series of images similar to the one shown in Fig. 10. The results on the left were obtained with a linear ramp preparation and the ones on the right were obtained with a Kaiser preparation. Both preparations were of length $p = 8$ (six echoes to discard). For each experiment the average signal of a circular region around the object and the two artifacts were obtained for each of the 32 different ω. The continuous lines are obtained from numerical simulation and fit the amplitude of the object (crosses) and the amplitude of the two artifacts (squares and diamonds).

performed in the same run, and using a ramping of length $p = 8$ (six echoes discarded), for $\beta = 0$ (linear ramp) and $\beta = 3$. This figure first shows that the fitting between the theoretical curves and the measures is not perfect, but is nevertheless convincing that the theory is probably true, knowing all the experimental uncertainties: there may still be some phase dispersion in the object due to resonant frequency inhomogeneity, as can be appreciated by the distortion of shape of the artifact in Fig. 10 when ω is around 0 or π. The figure clearly shows by comparison of the two ramps that the improvements to be expected from using the Kaiser window are indeed achieved.

5. Discussion

Ramping is not new, particularly for stabilization of FSE sequences. Alsop [22] noticing the improved signal obtained in [23] where a constant echo amplitude from the start of the echo train is obtained by variable profile RF pulses, proposed a downward ramp of the nutation angle (or downward ramp of the target echo amplitude); his idea was to transfer the initial magnetization from the axis $\vec{x}$ to a position parallel to the axis $\vec{n}$ (Alsop calls it the pseudo-steady state). The explanation why the downward ramp worked was not clear; some development based on the slow variation of the cycle rotation as used here would probably justify a large collection of downward ramps: when the nutation angle is high, close to 180° the fan picture of Fig. 2 or Fig. 4 has an aperture angle which is very small and the rotation axis is almost parallel to the $\vec{x}$ axis, where the magnetization lies at the start, and that for all precession angle ω. When slowly reducing the nutation angle the fan opens up and the magnetization follows the local rotation axis if the condition (14) is respected. One must realize that when ramping down as in the case of [22] for FSE, it is difficult to guarantee the respect of condition (14) when one is using selective pulses: if the condition is respected at the center of the slice, this does not imply that it is respected in another part of the slice, particularly as the borders where the nutation angle is small. Contrarily to that, the ramping up for SSFP stabilization proposed here or even in [8], is quite immune to a scaling. Indeed if one were to stabilize a SSFP train with a stable nutation angle $g\theta$ rather than θ one would find, using (25) and then (26), a stabilization sequence which will be itself multiplied by g! This will work in reality as long as the linear approximation is not broken. In that respect the Kaiser preparation with $\beta = 3$ resists more than the linear ramp and can still be used with a $p = 8$ and for a nutation angle $\theta = 2$. One can even ramp up to a $\theta = \pi$, obtaining an SSFP sequence which behaves like an FSE sequence in term or relaxation, if one admit to lengthen a bit the preparation period. In the other direction, both ramping up resist perfectly to a scaling down of the RF chain gain: the smaller the nutation angle the better they behave and thus there is no problem in using these ramping up with selective pulses. The effectiveness of the linear ramp up of [8] has recently been verified experimentally on phantoms and with volunteers in [24].

Another recent publication is also worth mentioning; it may seem that the FSE sequence has never been used in its refocused version. Actually yes; the TIDE sequence proposed in [25], and pertaining in appearance to the refocused SSFP sequence, can be seen as the refocused FSE sequence prepared by a (long) linear ramp-down of the nutation angle. Assuming that condition (14) is valid during this ramp-down the magnetization is left along the rotation axis as in Fig. 4. But at least for one half the ω this position is in reverse of the SSFP equilibrium it will reach after full relaxation (Fig. 5). This smooth transition from a refocused FSE sequence towards a refocused SSFP sequence may have interest for its own sake; but seen from the point of view of rapid refocused SSFP stabilization, it is efficient only in half of the possible ω. Besides, as with other previously proposed SSFP stabilization schemes [1], this demands a physical $T = \mathrm{TR}/2$ interval between two successive pulses and this may induce a lengthening of the TR. Also the use of high, close to π radian nutation angles at the start of the sequence may increase the Specific Absorption Rate and lengthen the time necessary to play the RF pulses.

Finally, a very recent article [26] tends to support the approach taken here to embed the two sequences FSE, and SSFP in the same framework by considering the cycle from center of precession period to center of precession period.

6. Conclusion

The results of [8] have been demonstrated and generalized. In the process of demonstrating the validity of the SSFP stabilization by ramping up, one has also demonstrated some results pertaining to FSE and proposed simplified equations to describe the relaxation processes which may be useful both for SSFP and FSE. The faster stabilization of SSFP may help obtaining other kind of image contrast.

Acknowledgments

The author wants to thank Franck Lethimonier and Jessica Dubois from Service Hospitalier Frederic Joliot (SHFJ) Orsay France for discussions which precipitated this work. Inside Applied Science Laboratory (ASL) of GE Medical System, the author was helped by Jason

Polzin (ASL East) who guided the author in the available bibliography and also implemented the proposed ramp in the product software, by Belinda Li (ASL East) who realized a first version of the experimental verification, Graeme McKinnon (ASL Milwaukee) furnished the software environment that the author used for programming the sequence, and finally Derek Shaw (ASL Europe) who took up the job of correcting this article. The last experimental verifications presented here were performed at SHFJ on a GE Signa 1.5 T which was financed by the Region Ile de France.

Appendix A

The perturbation theory of eigenvalues and eigenvectors will be used here in the classical mathematic sense [27], more than in the quantum physics approach [18] which deals with unitary operators. In case of no relaxation the vectors $v_1 = (\overrightarrow{v} + \mathrm{j}\overrightarrow{y})/\sqrt{2}$ and $v_2 = (\overrightarrow{v} - \mathrm{j}\overrightarrow{y})/\sqrt{2}$ are eigenvector of the 3D real matrix representing the rotation R with eigenvalue $\lambda = \exp(\mathrm{j}\Omega)$ and $\overline{\lambda} = \exp(-\mathrm{j}\Omega)$ respectively, and the vector $\overrightarrow{n}$ is eigenvector with eigenvalue 1. Let U the unitary matrix form by these vectors, for instance $U = [v_1|v_2|n]$ and Λ the diagonal matrix of eigenvalues $\mathrm{diag}(\lambda\overline{\lambda}, 1)$.

We use the fact that, with relaxation, the new matrix A is not very different from the original rotation:

$$A = (1 - O)R(1 - O),$$

$$A \simeq R - (OR + RO)$$

with $O = \mathrm{diag}(\omega_2 T, \omega_2 T, \omega_1 T)$, the variation $\mathrm{d}A = -(OR + RO)$ is a priori small if the repetition time is small in comparison to T_1, T_2. One will use a classical procedure to approximate the new eigenvalues and eigenvectors, similar to the stationary perturbation theory that is reminded rapidly. If one knows the eigenvector u_i of an operator A of order n with eigenvalues λ_i, $Au_i = u_i\lambda_i$. In which case one can express the operator A by

$$A = \sum_{i=1}^{n} \lambda_i u_i u_i^*. \tag{A.1}$$

To find out the new eigenvectors of $A + \mathrm{d}A$ one writes the new eigenvectors $u_i + \mathrm{d}u_i$ relative to a new eigenvalue $\lambda_i + \mathrm{d}\lambda_i$. One must have:

$$(A + \mathrm{d}A)(u_i + \mathrm{d}u_i) = (u_i + \mathrm{d}u_i)(\lambda_i + \mathrm{d}\lambda_i).$$

One supposes that the variations $\mathrm{d}u_i$ $\mathrm{d}\lambda_i$ are small and neglect second order terms in the previous equality (and making use of the fact that u_i is eigenvector of A):

$$A(\mathrm{d}u_i) + (\mathrm{d}A)u_i = (\mathrm{d}u_i)\lambda_i + u_i(\mathrm{d}\lambda_i).$$

One has n such equations $i = 1, \ldots, n$. Multiplying first by u_i^* each one of them (and using (A.1) and the orthogonality of the u_i):

$$u_i^*(\mathrm{d}A)u_i = \mathrm{d}\lambda_i. \tag{A.2}$$

Multiplying now the same equation by u_j^*:

$$\lambda_j u_j^*(\mathrm{d}u_i) + u_j^*(\mathrm{d}A)u_i = u_j^*(\mathrm{d}u_i)\lambda_i.$$

And if one express the variation of the eigenvector $\mathrm{d}u_i$ by a linear combination of the original eigenvector:

$$\mathrm{d}u_i = \sum_j b_{ij} u_j$$

one finds:

$$b_{ij} = \frac{u_j^*(\mathrm{d}A)u_i}{\lambda_i - \lambda_j}. \tag{A.3}$$

Applying this procedure to the present case turns out to be easy. One has $\mathrm{d}A = -(OR + RO)$ with R the original operator and O a diagonal, real matrix; in this condition one finds:

$$u_j^*(\mathrm{d}A)u_i = -(\lambda_i + \lambda_j)(u_j^* O u_i). \tag{A.4}$$

Then one finds from (A.2) with i corresponding to the rotation axis $\overrightarrow{n}$ ($\lambda = 1$)

$$\mathrm{d}\lambda = -2n^* O n.$$

Hence the new eigenvalue along this axis:

$$\lambda' = 1 - 2T * \ (\omega_1 n_z^2 + \omega_2 n_x^2).$$

This attenuation corresponds to a time interval $2T$, one can model this attenuation by a relaxation rate;

$$\omega_{\|} = \omega_1 n_z^2 + \omega_2 n_x^2.$$

In the same way considering (A.2) with v_1 corresponding to $\lambda = \exp(\mathrm{j}\Omega)$, one finds that the new eigenvalue is:

$$\lambda' = \mathrm{e}^{\mathrm{j}\Omega}(1 - 2v_1^* O v_1) = \mathrm{e}^{\mathrm{j}\Omega}(1 - y^{\mathrm{t}} O y - v^{\mathrm{t}} O v),$$

which after easy development leads to an equivalent relaxation rate:

$$\omega_{\perp} = \frac{\omega_2}{2} + \frac{\omega_1 n_x^2 + \omega_2 n_z^2}{2}.$$

The conjugate eigenvalue must stay conjugate (A is real) and thus corresponds to the same relaxation process. The operator A is a damped rotation in a plane with damping $\omega_{\perp}$ while the component along the axis is damped with the relaxation rate $\omega_{\|}$. The question is: does the axis of the rotation changed a lot? For accessing that let us use (A.3) with the index i corresponding to $\overrightarrow{n}$ and the index j corresponding to v_1:

$$b_{nv1} = (1 + \mathrm{e}^{\mathrm{j}\Omega})(v_1^* O n)/(1 - \mathrm{e}^{\mathrm{j}\Omega})(y O n)/(\mathrm{j}\tan(\Omega/2)),$$

$$b_{nv1} = -(1 + \mathrm{e}^{\mathrm{j}\Omega})(v_1^* O n)/(1 - \mathrm{e}^{\mathrm{j}\Omega})$$
$$= (v^{\mathrm{t}} O n)/(\mathrm{j}\sqrt{2}\tan(\Omega/2))$$

and the conjugate value for b_{nv2}. Finally:

$$n' = n + \frac{v^{t}On}{\tan(\Omega/2)}y$$

with $v^{t}On = (\omega_2 - \omega_1)T(n_x n_z)$, one has a component of the new rotation axis along the y axis which is:

$$n'_y = \frac{n_x n_z}{\tan(\Omega/2)} \times (\omega_2 - \omega_1)T.$$

The coefficient $K(\omega, \theta) = n_x n_z / \tan(\Omega/2)$ is a complicate function, but most evidently it will be large for small nutation angle θ and small precession angle ω where the rotation angle Ω is small. One simple rule is, for instance, the following: if one excludes around $\omega = 0$ and $\omega = \pi$ a segment of 0.175 rad ($\pm 10°$), one has always $K < 2$. As typically $\omega_2 T$ is in the order of 0.1 or below the rotation axis n' should not be tilted towards y by more than 10°. One will suppose that the axis of the (damped) rotation is the axis of the original rotation.

Hence, for studying the T_1 recovery one will suppose that the original eigenvector matrix U stays eigenvector matrix of the relaxed operator A and one will project all vector on this new basis. Taking into account the T_1 recovery during the precession periods, the magnetization recurrence equation between echo $k-1$ and k is (supposing $1 - E_1 \simeq \omega_1 T$):

$$M_k = ERE \times M_{k-1} + RE \times (\omega_1 T)z + (\omega_1 T)z.$$

Projecting this equation in the eigenvector frame by $M_k = Um_k$, $z = U\zeta$, and neglecting second order terms, one obtains:

$$m_k = \Lambda' m_{k-1} + \Lambda(\omega_1 T)\zeta + (\omega_1 T)\zeta. \tag{A.5}$$

This correspond to three decoupled first order systems. Two of them correspond to the perpendicular components y, v. But again if the rotation angle Ω is large enough there is one or more turns of rotation in one relaxation time $1/\omega_\perp$ and the component of the stationary magnetization along the y, v plane will be very small. In first approximation one will thus consider only the component along the rotation axis $\overrightarrow{n}$ which one find from the third line of (A.5). The component of $\overrightarrow{z}$ along $\overrightarrow{n}$ is n_z, and calling $\overline{m}$ the component of M_∞ along this same axis, one has

$$\overline{m}(1 - (1 - 2T * \ (\omega_1 n_z^2 + \omega_2 n_x^2))) = 2(\omega_1 T)n_z,$$

$$\overline{m} = \frac{\omega_1}{\omega_1 n_z^2 + \omega_2 n_x^2} n_z.$$

Appendix B

In [28], Hennig admitted not being able to demonstrate that the signal of FSE (or CPMG) sequence is $\sin(\theta/2)$.

Here is one demonstration following Fig. 4 and Eq. (8). The original magnetization along x is first projected 'by phase dispersion' along $\overrightarrow{n}$, with a magnitude n_x; to calculate the signal it generates one has to project that magnetization on x, hence the original magnetization at precession angle ω gives rise to a signal increment $n_x^2(\omega)$. The global signal is then

$$S = \int_{-\pi}^{\pi} n_x^2(\omega)\,\mathrm{d}\omega$$

or

$$S = \int \mathrm{d}\omega s^2/(s^2 + c^2 \sin^2\omega)$$

$$= \int (1 + \tan^2\omega)\mathrm{d}\omega/(1 + \tan^2\omega/s^2),$$

or

$$S = \int_{-\infty}^{+\infty} \frac{\mathrm{d}u}{1 + u^2/s^2}$$

with $u = \tan\omega$, and now with $v = u/s$ and $v = \tan\alpha$:

$$S = s\int_{-\infty}^{\infty} \frac{\mathrm{d}v}{1 + v^2} = s.$$

References

[1] M. Deimling, O. Heid, Magnetization prepared true FISP imaging, in: Proceedings Second SMR Scientific Meeting, San Francisco, CA, 1994, p. 495.

[2] A. Oppelt, R. Grauman, H. Fischer, W. Hartl, W. Shajor, FISP—a new fast MRI sequence, Electromedica 54 (1986) 15–18.

[3] O. Heid, True FISP cardiac fluoroscopy, in: Proceedings Fifth Annual Meeting ISMRM, Vancouver, 1997, p. 320.

[4] J. Bundy, O. Simonetti, G. Laub, J.P. Finn, Segmented true FISP cine imaging of the heart, in: Proceedings Seventh Annual Meeting ISMRM, Philadelphia, 1999, p. 1282.

[5] B.A. Hargreaves, S.S. Vasanawala, J.M. Pauly, D.G. Nishimura, Characterization and reduction of the transient response in steady-state MR imaging, Magn. Reson. Med. 46 (2001) 149–158.

[6] B.A. Hargreaves, J.M. Pauly, D.G. Nishimura, Shinnar-le roux design for steady-state manipulation sequences, in: Proceedings Tenth Scientific Meeting ISMRM, Honolulu, 2002, p. 379.

[7] J. Pauly, P. Le Roux, D. Nishimura, A. Macovski, Parameter relations for the Shinnar–Le Roux selective excitation pulse design algorithm, IEEE Trans. Med. Imaging 10 (1991) 53–65.

[8] D.G. Nishimura, S. Vasanawala, Analysis and reduction of the transient response in SSFP imaging, in: Proceedings Eight Annual Meeting ISMRM, Denver, 2000, p. 301.

[9] M. Haacke, R.W. Brown, M.R. Thompson, R. Venkatesan, Magnetic resonance imaging, Wiley–Liss, New-York, 1999.

[10] K. Scheffler, O. Heid, J. Hennig, Magnetization preparation during the steady state: Fat-saturated 3d true FISP, Magn. Reson. Med. 45 (2001) 1075–1080.

[11] A. Messiah, Quantum Mechanics, Dover, New York, 2000.

[12] E. Jaynes, Matrix treatment of nuclear induction, Phys. Rev. 98 (1954) 1099–1105.

[13] A.L. Bloom, Nuclear induction in inhomogeneous fields, Phys. Rev. 98 (1954) 1105–1111.

[14] P.L. Roux, Non-cpmg fast spin echo with full signal, J. Magn. Reson. 155 (2002) 278–292.

[15] C.P. Slichter, Principles of Magnetic Resonance, Springer, New York, 1992.

[16] J. Hennig, T. Kluge, K. Scheffler, Multiecho sequences with variable refocusing flip angles: optimization of signal behaviour using smooth transition between pseudo steady states (traps), in: Proceedings Tenth Scientific Meeting ISMRM, Honolulu, 2002, p. 2356.
[17] M. Garwood, L. Delabarre, The return of the frequency sweep: Designing adiabatic pulses for contemporary NMR, J. Magn. Reson. 153 (2002) 155–177.
[18] L.I. Schiff, Quantum Mechanics, McGraw-Hill, London, 1969.
[19] J.F. Kaiser, Non recursive digital filter design using the i0-sinh window function, in: Proceedings 1974 IEEE Int. Symp. Circuits Systems, 1974, pp. 20–23.
[20] D.F. Elliot, Handbook of Digital Signal Processing, Engineering Applications, Academic Press, San Diego, 1987.
[21] F.H. Epstein, D. Kim, E. McVeigh, Reducing signal oscillations during the approach to steady state in true FISP using partial dephasing, in: Proceedings Ninth Annual Meeting ISMRM, Glasgow, 2001, p. 1786.
[22] D.C. Alsop, The sensitivity of low flip angle rare imaging, Magn. Reson. Med. 37 (1997) 176–184.
[23] P. Le Roux, S. Hinks, Echoes stabilization in FSE sequences, Magn. Reson. Med. 30 (1993) 183–191.
[24] V.S. Deshpande, Y.-C. Chung, Q. Zhang, S.M. Shea, D. Li, Reduction of transient signal oscillations in true-FISP using a linear flip angle series magnetization preparation, Magn. Reson. Med. 49 (2003) 151–157.
[25] J. Hennig, O. Speck, K. Scheffler, Optimization of signal behavior in the transition to driven equilibrium in steady-state free precession sequences, Magn. Reson. Med. 48 (2002) 801–809.
[26] K. Scheffer, J. Hennig, Is true FISP a gradient-echo or a spin-echo sequence? Magn. Reson. Med. 49 (2003) 395–397.
[27] G.H. Golub, C.F. Van Loan, Matrix computations, The Johns Hopkins University Press, Baltimore, 1990.
[28] J. Hennig, Echoes—how to generate, recognize, use or avoid them in MR-imaging sequences, part i, Concepts in Magn. Reson. 3 (1991) 125–143.